The Cryosphere, 5, 67–79, 2011
www.the-cryosphere.net/5/67/2011/
doi:10.5194/tc-5-67-2011

The Cryosphere

Modeling the temperature evolution of Svalbard permafrost during the 20th and 21st century

B. Etzelmüller[1], T. V. Schuler[1], K. Isaksen[2], H. H. Christiansen[3,1], H. Farbrot[1], and R. Benestad[2]

[1]Department of Geosciences, University of Oslo, Norway, P.O. Box 1047, Blindern, 0316 Oslo, Norway
[2]Norwegian Meteorological Institute, P.O. Box 43, Blindern, 0313 Oslo, Norway
[3]Arctic Geology Department, The University Centre in Svalbard (UNIS), P.O. Box 156, 9171 Longyearbyen, Norway

Received: 24 August 2010 – Published in The Cryosphere Discuss.: 4 October 2010
Revised: 30 December 2010 – Accepted: 21 January 2011 – Published: 4 February 2011

Abstract. Variations in ground thermal conditions in Svalbard were studied based on measurements and modelling. Ground temperature data from boreholes were used to calibrate a transient heat flow model describing depth and time variations in temperatures. The model was subsequently forced with historical surface air temperature records and possible future temperatures downscaled from multiple global climate models. We discuss ground temperature development since the early 20th century, and the thermal responses in relation to ground characteristics and snow cover. The modelled ground temperatures show a gradual increase between 1912 and 2010, by about 1.5 °C to 2 °C at 20 m depth. The active layer thickness (ALT) is modelled to have increased slightly, with the rate of increase depending on water content of the near-surface layers. The used scenario runs predict a significant increase in ground temperatures and an increase of ALT depending on soil characteristics.

1 Background and objectives

Changes in the spatial extent and temperatures of permafrost are generally taken as consequences of climate change (e.g. Lachenbruch and Marshall, 1986). Permafrost is continuous in the parts of the high-arctic archipelago of Svalbard not covered by glaciers (75–82° N) (e.g. Humlum et al., 2003; Liestøl, 1977). The location of Svalbard in the northern part of the warm North-Atlantic ocean current makes its climate especially sensitive to atmospheric and oceanic changes (e.g. Aagaard and Carmack, 1989). Accordingly, a 4–6 °C warming and +5% precipitation increase are projected by Global Circulation Models (GCM) for Svalbard by 2100 according to the SRES A1b emission scenario (Benestad, 2005; ACIA, 2005). Since permafrost inhibits prominent groundwater flow and stabilizes frozen, unconsolidated sediments, the degradation of permafrost is likely to have wide influences on processes shaping the physical and human environment (e.g. Williams and Smith, 1989; French, 1996). Temperature profiles through the permafrost reflect to some extent the history of the ground surface temperature, which, in turn, is closely coupled to air temperature, vegetation and snow cover (e.g. Lachenbruch and Marshall, 1986; Goodrich, 1982). A Svalbard ground surface temperature reconstruction, based on a heat conduction inversion model, indicated a warming of the permafrost surface of 1.5 °C ± 0.5 °C over the last 6–8 decades (Isaksen et al., 2000) in the bedrock-dominated site of Janssonhaugen. Between 1999 and 2009 the permafrost has warmed there by 0.9 °C at 20 m depth. Significant warming is detectable down to at least 60 m depth, and the present decadal warming rate at the permafrost surface (ca. 2 m depth) is in the order of $0.07°\ \mathrm{C\,a^{-1}}$, with indications of accelerated warming during the last decade (Isaksen et al., 2007b).

In this paper, we use ground temperatures collected from five boreholes, most of which were established during the International Polar Year project TSP-NORWAY (Permafrost Observatory Project: a contribution to the Thermal State of Permafrost in Norway and Svalbard; Christiansen et al., 2010) to calibrate an 1-D heat conduction model and establish statistical relationships between local ground surface temperatures (GST) and surface air temperatures (SAT) at a nearby meteorological station. This framework enables the reconstruction of borehole temperatures since 1912 using a historical record of air temperature. Furthermore, we assess

Correspondence to: B. Etzelmüller
(bernde@geo.uio.no)

Fig. 1. Location of the studied borehole sites in Svalbard (inlet map) in the Nordenskiöldland Permafrost Observatory (see also Juliussen et al., 2010). The selected sites for this study on the Nordenskiöld peninsula are Endalen, Janssonhaugen, Gruvefjellet and Kapp Linné.

the possible future permafrost conditions and the related uncertainties, by using downscaled air temperature projections from an ensemble of GCMs for the 21st century (Benestad, 2008, 2011).

2 Permafrost and air temperature observations

We used four locations studying five boreholes, situated in the central and western part of Svalbard, and covering a roughly west-east transect from the most maritime west-coast at Kapp Linné to the inland in the Longyearbyen/Adventdalen area (Fig. 1, Table 1). An overview of location, landforms, stratigraphy and detailed instrumentation of these sites is given by Christiansen et al. (2010). Site information particularly relevant for this study is given below and in Table 1. Three boreholes were drilled in bedrock with little sediment cover and thin snow cover (Janssonhaugen, Kapp Linné, BH 1), whereas the other boreholes have a considerable sediment cover consisting of 1 m regolith at Gruvefjellet, a solifluction sheet with 6–7 m diamicton (Endalen) and 7 m of beach ridge sandy to pebbly sediments at Kapp Linné BH 2. The two boreholes at Kapp Linné are less than 100 m apart, differing only by the amount of sediment cover. At all boreholes ground temperature is recorded automatically, usually in 1 or 6 h intervals, with the longest series from Janssonhaugen (Isaksen et al., 2000). On-site meteorological observations are available from Janssonhaugen, Kapp Linne and Gruvefjellet.

3 Methodology

3.1 Historical meteorological data

West Spitsbergen has three official meteorological stations with long time series, Svalbard Airport (close to Longyearbyen, 5 m a.s.l.), Isfjord Radio (Kapp Linné, 10 m a.s.l.) and Ny-Ålesund (Fig. 1) (5 m a.s.l.). Mean annual air temperature (MAAT) for the standard normal period 1961–1990 for Svalbard Airport is −6.7 °C, and mean annual precipitation is 190 mm. The Isfjord Radio station shows more maritime conditions, having higher precipitation (480 mm) and mean surface air temperature is −5.1 °C. The temperature variability is highly correlated between the three stations ($r^2 > 0.9$), with the largest differences between Svalbard Airport and Isfjord Radio. The mean annual lapse rates between the Longyeardalen valley bottom (app. 60 m a.s.l.) and the Gruvefjellet meteorological station (464 m a.s.l.) was 0.0062 °C m^{-1} (2001-2010). There are major inter-seasonal differences, with lapse rates ranging from +0.01 °C m^{-1} during end of winter/early spring (May–June) to −0.01 °C m^{-1} during winter inversions.

The homogenised monthly temperature series of Svalbard Airport (1912 – present) (Nordli and Kohler, 2004) is a composite of several shorter series of measurements carried out at a few nearby sites. All shorter series are adjusted to the current Svalbard Airport meteorological station (established in 1975). The beginning of the series coincides with the end of the Little Ice Age in Svalbard (Fig. 2). Since 1912

Table 1. Calibration parameters used for ground temperature modelling. Thermal conductivity and bedrock density were selected from published literature and fine-adjusted during calibration. Effective diffusivity was estimated based on the measured ground temperatures

Borehole name and elevation	Layers (lower boundary) m	Thermal conduc. $Wm^{-1}K^{-1}$	Density $kg\,m^{-3}$	Effective diffusivity $m^2\,s^{-1}$	Water/ice content vol %	Ground thermal heat flow Wm^{-2}	Calibration (validation in curs.) time period	Total depth of boreh. m	Stratigraphy	Bedrock type	Logger info
Endalen (53 m a.s.l.)	<1 2 4 7 >7	1.0 1.2 1.5 1.7 2.2	1500 1600 1800 2000 2300	1.17×10^{-7} 10×10^{-7} 9.8×10^{-7}	9 12 7 5 3	0.065	17 Sep 2008– 10 Feb 2010	20	Solifluction sheet (ca. 5–7 m), weathered bedrock (ca. 2 m) (diamicton, inter-layered with finer material, scattered blocks)	Sandstones, siltstones and shale (Middle Jurassic)	YSI 44006 thermistors ($\pm0.02\,^\circ$C) Campbell logger
Gruvefjellet (464 m a.s.l.)	<0.8 1.4 2.4 4 >4	1.0 1.2 1.3 1.9 2.1	1300 1500 1900 2100 2300	0.7×10^{-7} 14×10^{-7}	5 12 8 4 3	0.065	15 Mar 2008– 10 Feb 2010	5	Regolith (0.8 m)	Sandstones, shale (Palaeocene to Eocene-Tertiary)	Campbell logger, RST (c) thermistor ($\pm0.1\,^\circ$C)
Kapp Linné BH1 (10 m a.s.l.)	<3 6 10 14 >14	2 2.5 2 2.8 2.8	2200 2300 2700 2700 2700	2.6×10^{-7} 19×10^{-7} 24×10^{-7}	3.5 2.5 1.5 1 1	0.065	23. Sep 2008– 18. Mar 2010	30	Bedrock	Schist and carbonates (pre-Devonian)	YSI 44006 thermistors ($\pm0.02\,^\circ$C) Campbell logger
Kapp Linné BH2 (10 m a.s.l.)	<2 5 6.5 15 >15	0.6 1.5 1.2 2.6 2.8	1000 1500 1200 2500 2700	1.4×10^{-7} 7.8×10^{-7} 12×10^{-7}	1.5 9 3 2 2	0.065	23 Sep 2008– 18 Mar 2010	40	Litoral beach ridge sediments (6–7 m) (2 m pebbles 2.5 m sand/silt 1.5 m pebbles)	Shiest and carbonates (pre-Devonian)	YSI 44006 thermistors ($\pm0.02\,^\circ$C) Campbell logger
Jansson -haugen (270 m a.s.l.)	<1 3 >3	1.6 1.8 2.2	2300 2300 2300	2.1×10^{-7} 9.3×10^{-7}	6 5 3	0.065	1 Jan 2000– 21 Dec 2004 1 Jan 2005– 27 Feb 2009	102	Bedrock	Sandstone, with some thin layers of shale (Middle Jurasic)	YSI 44006 thermistors ($\pm0.02\,^\circ$C) Campbell logger

annual mean temperatures have changed by about 4 °C, from ca. −8 °C at the end of the last century to −4 °C today. The MAAT has varied between −8 °C and −5 °C (Fig. 2) between 1920 and ca. 1960. Since the late 1980s MAAT has again increased. The main characteristics of Svalbard's air temperature development since the end of the Little Ice age are the cold decades in the 1910s, 1960s and partly the 1980s, and the warm spell around the 1930s and the 1950s. Since 1990 a positive trend is seen. Inter-annual variations are large, and are mostly driven by variations in winter temperatures, while summer temperatures exhibit little variation. This pattern clearly demonstrates the maritime setting of the archipelago and the influence of sea ice cover (cf. Førland and Hannssen-Bauer, 2003).

3.2 GCM scenario data for Svalbard Airport

For Svalbard Airport, monthly air temperatures covering the 20th and 21st Centuries are available (Fig. 2) based on empirically statistically downscaling an ensemble of GCM scenarios (Benestad, 2008, 2011; Isaksen et al., 2007a). The empirical-statistical downscaling consisted in a step-wise screening multiple regression between the local series (predictand) and the surrounding large-scale (predictor) temperature patterns. Large-scale monthly mean surface air temperature (SAT) was used as predictor to derive the local monthly temperature for Svalbard Airport.

The predictors were represented in form of common empirical orthogonal functions (Sengupta and Boyle, 1998; Benestad, 2001), which use principal component analysis (Strang, 1988) to describe how different spatial structures vary in time. The calibration and projection were carried out for each of the calendar months separately, and subsequently assembled for the whole year.

The empirical-statistical downscaling provides some indication about how well the local temperature can be reproduced by the predictors, in terms of the analysis of variance associated with multiple regression (Wilks, 1995). The resulting r^2-statistics are highest for the autumn, spring, and winter months (January: 0.94; February: 0.81; March: 0.91; April: 0.91; May: 0.89; September: 0.90; October: 0.96; November: 0.95; December: 0.95) and lowest in summer (June: 0.53; July: 0.67; August: 0.59). Furthermore, the regression weights provide further diagnostics (not shown) that can be compared with correlation maps for evaluation. The reasonably smooth variation in the trend estimates over the season (not shown) suggests that the scenarios are not spurious. The strongest warming was estimated for the

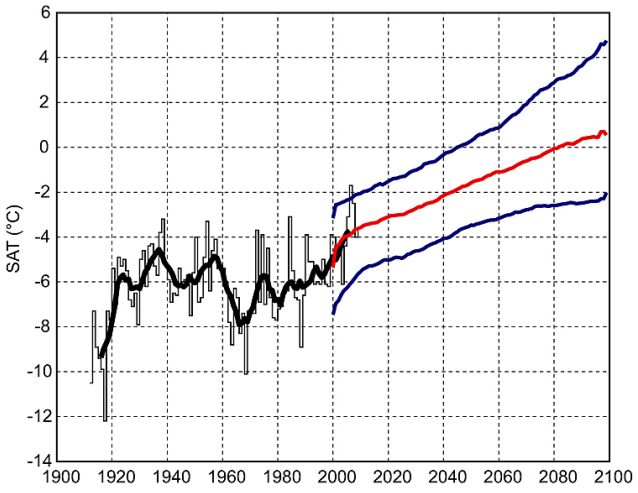

Fig. 2. The official mean annual surface air temperature record at Svalbard Airport. The bold line represents a 7 year Gauss-filtered series of MAAT with three standard deviations. The distribution of the 32 downscaled future scenarios are displayed as percentiles between 2000 and 2100, where the red line is the median and the blue lines represent the 10% and 90% percentiles, respectively. Note that the observed annual temperature closely matches the scenario median in the 10 year overlap period, with the extreme year of 2006/2007 being outside even the 90% percentile (Isaksen et al., 2007a).

winter months (+0.6–0.8°C/decade) while the weakest trends (+0.05–0.2°C/decade) were estimated for the summer, for which, however, the r^2-estimates are lowest. Hence, the downscaling analysis may underestimate the summer-time warming. The weaker performance for the summer season can be explained in terms of a weaker link between local temperatures and the sea-ice extent (Benestad et al., 2002). Climate models do often have problems in correctly describing sea-ice (Stroeve et al., 2007).

The Svalbard Airport temperature data was taken from the station climate archive of the Norwegian Meteorological Institute, and the calibration of the downscaling models was based on the 40-years reanalysis of the European Centre of Medium-range Weather forecast (ERA40; Uppala et al., 2005). The set of global climate model simulations was from the multi-model World Climate Research Programme (WCRP) Coupled Model Intercomparison Project (CMIP3; Meehl et al., 2007), all of which followed the Special Report Emission Scenario (SRES) A1b (in which atmospheric CO_2 reaches 720 ppm by 2100). These climate scenarios are documented in the Intergovernmental Panel on Climate Change (IPCC) Assessment Report 4 (AR4; Solomon et al., 2007). The Arctic Climate Impact Assessment (ACIA, 2005) provides a more detailed analysis of the Arctic, for which an enhanced greenhouse gas warming is expected to be more pronounced than elsewhere on the planet.

3.3 Ground temperatures

The ground temperatures in the boreholes vary mainly according to elevation, distance to sea, land form/sediment types, and by variations in snow cover and near surface ice- and water content. In the year from summer 2008 to summer 2009, boreholes had mean annual ground temperatures (MGT) at 15 m depth ranging from −3.2 °C at the west coast at Kapp Linné and in the valley bottom of Endalen to −5.4 °C and ca. −6 °C further inland in sedimentary valley innfill and at higher elevation at Janssonhaugen (Fig. 3e–h) (Christiansen et al., 2010). The Endalen borehole has higher ground temperatures, which is related to the snow cover, and wetter summer ground conditions due to receiving runoff from upslope areas (Christiansen et al., 2010). The active layer thicknesses (ALT) varied between around 2.5 m in the bedrock sites of Kapp Linné and Jannsonhaugen to close to 1 m in the Endalen site and Gruvefjellet sites (Christiansen et al., 2010).

At each site ground surface temperature (GST) was measured, either by a separate data logger in ca. 5 cm depth or by the first thermistor located at 0 m depth in the borehole. The records from Kapp Linné, Gruvefjellet and Janssonhaugen reveal a relatively close coupling between GST and SAT, while at Endalen, coupling is complicated due to more pronounced snow and vegetation covers and their associated insulating properties (Fig. 3d).

We calculated the ratios of annual sums of freezing or thawing degree days of GST to those of SAT, referred to as n-factors n_T and n_F, respectively (e.g. Smith and Riseborough, 2002). The n-factors were calculated over the same period as the ground temperature measurements, which is >10 years for the Janssonhaugen site (2000–2010) and >2 years for the other sites (2008–2010). For Janssonhaugen the n-factors were practically constant, with variations of 1.05 to 1.07 during freezing and 1.12 to 1.19 during thawing. For Gruvefjellet and Kapp Linné a similar near constant value was calculated (Kapp Linné 1.00, Gruvefjell 1.18 for the thawing factor, n_F was between 0.95 and 1). For Endalen, the freezing factor in 2009/2010 was slightly lower (0.78 to 0.74), while the thawing factor increased from 0.83 to 0.93. Hence, for the non-vegetated sites, the thawing n-factor $n_T \geq 1$ is characteristic for equal or warmer summer conditions at the ground surface than at screen level (2 m above ground). At the Endalen site, n_T was considerable lower, equivalent to lower summer GST than summer SAT. As the freezing n-factor (n_F) depends mainly on snow cover, $n_F < 1$ indicates a weak coupling between GST and SAT due to the insulating effect of the snow cover. Here, the observed inter-annual variation of the freezing factor will of course depend on the snow cover timing, duration and quantity. For the more open wind-exposed sites, little changes in snow cover in the future might be expected.

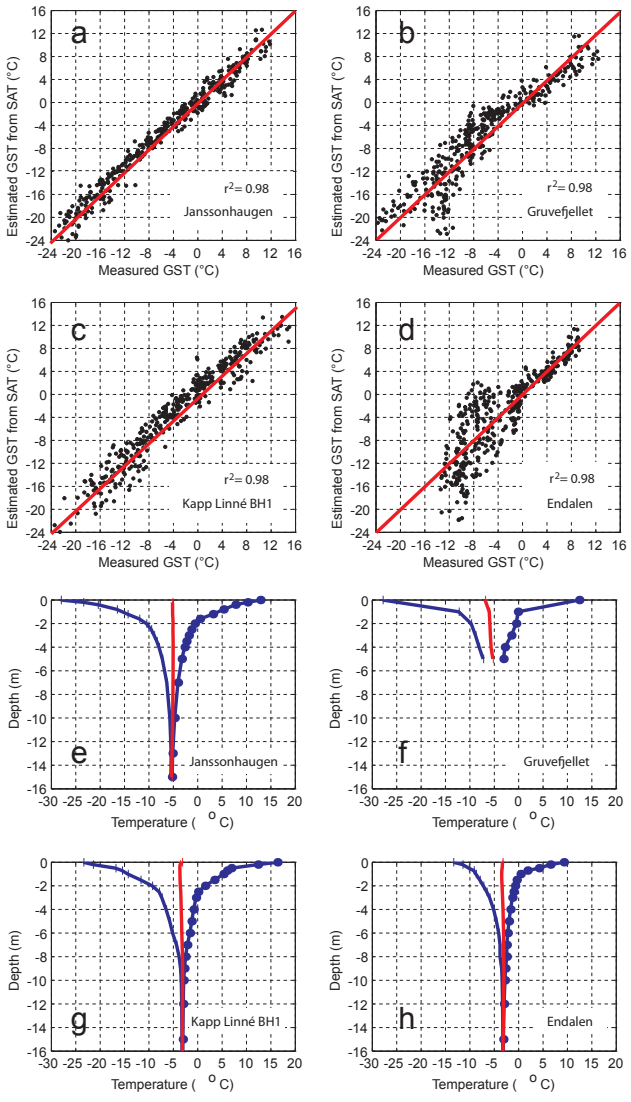

Fig. 3. (a–d) Measured ground surface temperature (GST) plotted against estimated GST based on the surface air temperature (SAT) from Svalbard Airport and a n-factor based transfer function. Only the Endalen site showed a significant effect of snow cover during winter, resulting in a lower but still satisfying r^2 of above 0.75. At the other sites, modelled and observed GST agree well ($r^2 > 0.87$). **(e–h)** The red lines represent measured mean ground temperature at various depths for the 2008/2009 period. The envelope of maximum and minimum temperatures is shown by the blue lines. Thermistor locations are indicated by the solid circles.

These n-factors were then used to derive GST series for each site from the long-term SAT series (1912–2009) and from the multi-model ensemble SAT scenarios (2001–2100) for Svalbard Airport. This was achieved by first adjusting the SAT from Svalbard Airport to the elevation of the considered site utilizing a simple regression to the sites with meteorological information (Kapp Linné, Janssonhaugen, Gruvefjellet), with a $r^2 > 0.9$, or a lapse rate (Endalen). Subsequently, we derived the GST for each site based on the n-factors. During the calibration period (see below) we achieved a $r^2 > 0.75$ for all sites (Fig. 3a–d).

3.4 Heat flow model

The subsurface temperature distribution was simulated by numerically solving the transient 1-D heat equation for non-constant coefficients (see also Farbrot et al., 2007 for more details):

$$\rho\, c \frac{\partial T}{\partial t} = -\frac{\partial}{\partial z}\left(k \frac{\partial T}{\partial z}\right) \quad (1)$$

(Williams and Smith, 1989). As boundary conditions, we prescribe time series of GST and the geothermal heat flux $Q_{\mathrm{geo}} = 65\,\mathrm{mW\,m^{-2}}$ at depth (Isaksen et al., 2000) (see also explanation on page 1885). The thermal properties of the ground are described by density ρ, thermal conductivity k and heat capacity c. The presence of water and ice in the substrate has a twofold effect on the thermal properties. First, the thermal properties of water and ice are different to those of the matrix, and we consider effective values as a linear mixture of values for the substrate and the corresponding ones for the volumetric content of water or ice, depending on the temperature conditions. Secondly, the water content affects the thermal properties during the phase transitions. During freezing or thawing, the latent heat associated with these phase changes is released or consumed, respectively. In our model runs, we apply an apparent heat capacity to consider the change of latent heat L due to phase changes of the pore water within a small temperature interval of $\pm 0.1\,^{\circ}\mathrm{C}$ around the freezing temperature (e.g. Wegmann et al., 1998)

$$c_{(\mathrm{T})} = c_0 + \frac{L}{(T_2 - T_1)} \quad (2)$$

Further, any effects of heat advection related to water flow in the active layer are neglected in our modelling. The heat conduction equation (Eq. 1) was discretized along the borehole depth using finite differences and subsequently solved by applying the method of lines.

3.5 Calibration and model initialisation

To achieve a first impression of the parameter space, the mean apparent thermal diffusivity (κ_a) was determined for the different layers at the borehole locations following Williams and Smith (1989):

$$\kappa_a = m^2/p \quad (3)$$

where m is the slope of a linear fit to the natural logarithm of the maximum amplitude $A(z)$ versus depth, assuming that the period p is one year. Effective diffusivities ranged from around $0.7\text{–}2.6 \times 10^{-7}\,\mathrm{m^2\,s^{-1}}$ in the surface sediment layers to $10\text{–}19 \times 10^{-7}\,\mathrm{m^2\,s^{-1}}$ in sedimentary bedrock (Table 1).

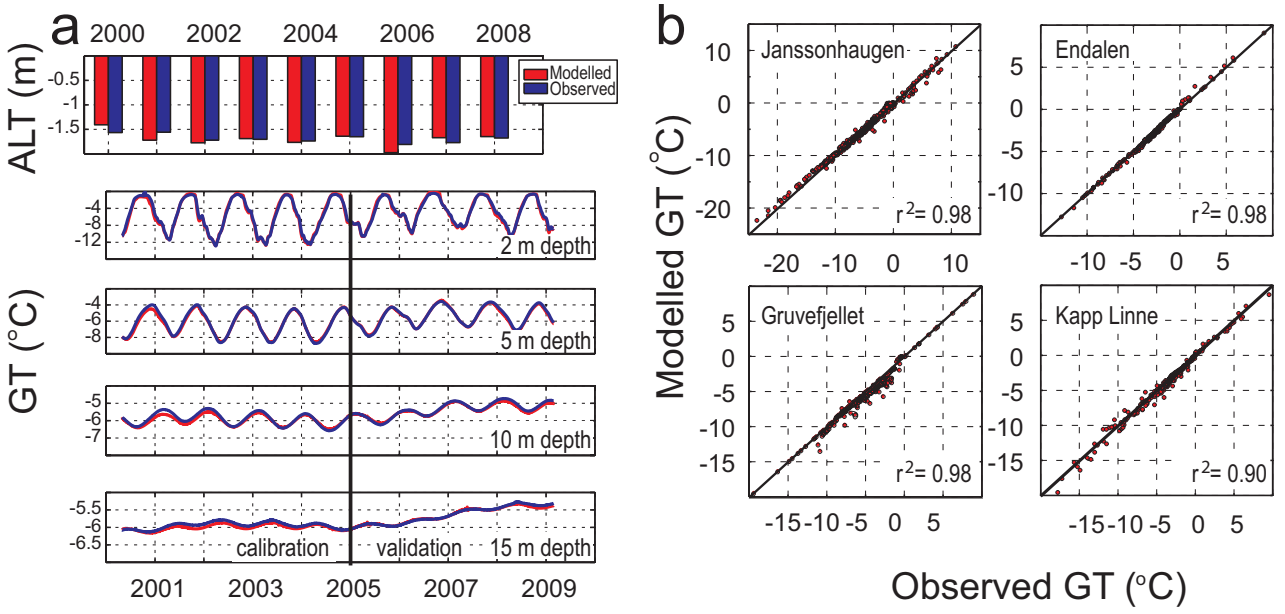

Fig. 4. (a) Calibration and validation plots for Janssonhaugen, comparing active layer thickness (ALT, upper) and temperature development in different depths (lower, note different scaling of GT axes). **(b)** Scatter plots of measured vs. modelled ground temperatures at the various study sites.

All sites modelled in this study were calibrated to closely reproduce measured ground temperatures (Fig. 4). Each calibration was started from the observed distribution of ground temperatures, at least one month after drilling, when thermal disturbance from the drilling was assumed to be negligible. The model domain was 150 m discretized in constant steps of 0.1 m. Thermal conductivity and bedrock density values were selected from published literature and fine-adjusted during calibration (Table 1). Main calibration parameter was the water/ice content, influencing the effective damping and retardation of the temperature signal in the active layer. The calibration period was between 500 and 680 days (see Table 1). The calibrated models show good correspondence between observed and modelled temperatures yielding r^2-values of above 0.9 (Fig. 4). However, the Gruvefjellet site is most weakly constrained because of coarsely-spaced sensors and lacking information below 5 m.

For Janssonhaugen, ground temperature has been measured since May 1998, and local meteorological records are available since spring 2000. At this location we divided the dataset into a calibration (May 2000–May 2005) and a validation period (June 2005–April 2009) (Fig. 4a). The model performed well in closely reproducing measured temperature time series at various depths as well as the active layer thickness (Fig. 4a).

To reproduce a realistic temperature distribution at depth below the lowermost sensor (Jansonhaugen 100 m, otherwise ∼5–40 m), the models were initialised using colder conditions than today. For all boreholes we used SATs derived from the mean MAAT 1912–1922 from Svalbard Airport (−8 °C) and superimpose a harmonic function to mimic the seasonal variation of SAT. The amplitude of that variation was derived from the observed variations of the respective SAT records (typically $r^2 > 0.8$). The models were then spun up over 200 years or until steady state was reached.

4 Results

4.1 Historical ground thermal regime

Janssonhaugen is the best calibrated and validated site, as deeper ground temperatures are available below 50 m. Our model was forced using site-specific GST series (Fig. 3a–d) which in turn were derived from the instrumental record from Svalbard Airport (Fig. 2). Model results show for all sites a 1–3 °C permafrost temperature increase over the last century at 10 m depth; at 50 m depth ground temperatures have increased by <1 °C (Fig. 5a–b), and at 100 m depth only minor variations were modelled. The largest changes were modelled at Kapp Linné BH1, presumably because of the assumed low water/ice content and the associated low thermal buffering capacity (Fig. 5). At all sites the modelled ALT shows some inter-annual variation but no clear trend between ca. 1920 and ca. 1990, later more substantial warming have led to an increase in ALT (Fig. 5c–d). The simulated ALT increase since the 1990s is between 1.25 cm a^{-1} (Gruvefjellet) to 3 cm a^{-1} (Kapp Linné BH1 and Janssonhaugen). For the sediment-rich locations Endalen and Kapp Linné BH2, the change rates in ALT were similar with 1.25 cm a^{-1} and 2.2 cm a^{-1}, respectively (Fig. 5c).

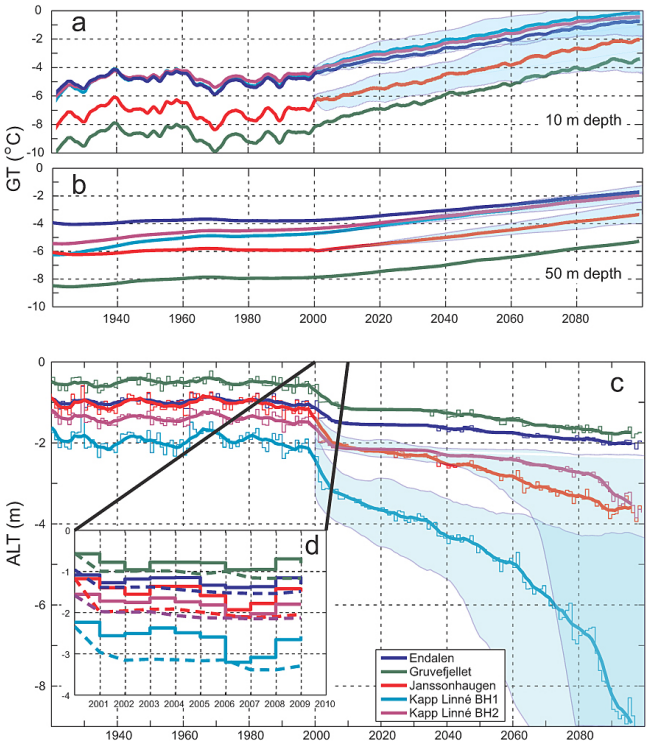

Fig. 5. Evolution of ground temperatures and ALT 1912–2099. Until 2000 the model was driven by instrumental data, from 2000 results of the scenario runs are shown. All series were smoothed with a 24 months Gaussian filter. **(a)** Ground temperature development since 1912 in 10 m and **(b)** 50 m depth. The shaded areas illustrate the spread of model results between the 10% and 90% percentiles. The shaded area is only given for the Kapp Linné BH1 and the Janssonhaugen site. **(c)** Modelled maximum active layer thickness during the same period. The shaded area illustrates the modelled ALT spread for the 10% and 90% percentile scenario results for the Kapp L. BH1 site (gray, bedrock site) and the Kapp L. BH2 (yellow, sediment-covered site). **(d)** Comparison between modelled ALT based on instrumental data (solid line) and median GCM scenario run (stippled line) in the overlap period 2000–2010.

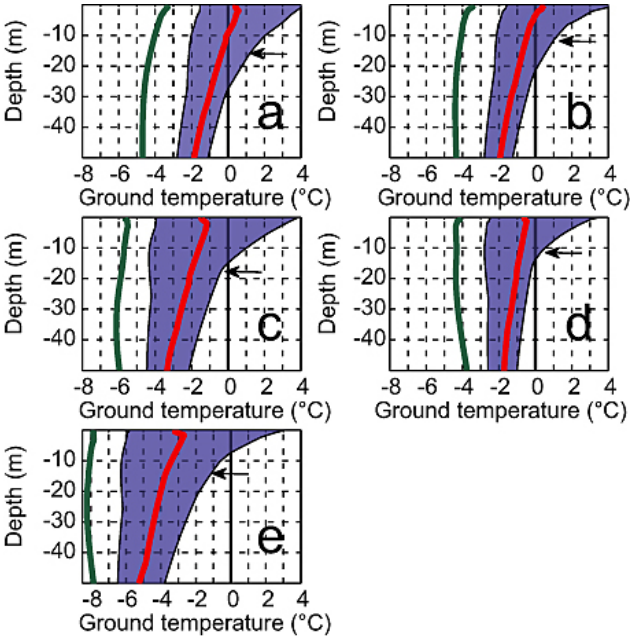

Fig. 6. Predicted future evolution of permafrost temperatures. **(a)** Kapp L. BH1, **(b)** Kapp L. BH2, **(c)** Janssonhaugen, **(d)** Endalen, **(e)** Gruvefjellet. The green lines represent the start conditions, either measured (Janssonhaugen) or derived from the historic modelling based on instrumental data from January 2000 (all other sites). The red line is the median of all scenario results, the shaded polygon denotes minimum and maximum GT from the scenario runs. The ZAA is indicated by arrows and is situated between 10 and 20 depth.

4.2 Future ground thermal regime

All together 32 individual SAT scenarios derived from downscaling a multi-model GCM ensemble were used to further derive GST series for the individual borehole locations, which in turn provided the surface boundary conditions to drive the ground heat conduction models. For Janssonhaugen, the model was initialised from observed January 2000 temperatures, and the others were started from the end of the subsurface temperature reconstruction described above. The uncertainty of the future evolution is demonstrated by the spread of the individual SAT scenarios within the ensemble (Figs. 2 and 6). Here, we present the median of the different results to provide a balanced picture of the potential future development of the ground thermal regime along with the 10% and 90% percentiles to indicate the uncertainty for two of the sites (Figs. 5 and 6). The climate scenario forcing revealed the following major effects of the permafrost thermal state:

1. The expected SAT warming during the 21st century will result in a significant warming (ca. +4 °C) in the near-surface (<10 m depth) layers (Figs. 5 and 6).

2. The spread of the individual temperature scenarios at the depth of zero annual amplitude (ZAA) varies between 5 °C and 2.5 °C, depending on ice/water content and distance to the 0 °C isotherm (Fig. 6).

3. Warming rates are efficiently reduced where the temperature is close to 0 °C and where ice is present due to the consumption of latent heat for melting.

4. The median ground temperatures at the depth of ZAA is suggested to increase by 2–4 °C over the period 2000–2100.

5. Over the same period, ALT increases at all sites, the magnitudes of the modelled increase depend on GST and ground characteristics. While ALT roughly doubles at Gruvefjellet (+0.7 m), Endalen (+1 m), Kapp Linné

BH2 (+2.5 m) and Janssonhaugen (+2 m), the increase is more pronounced at Kapp Linné BH1 (+8 m) and may lead to the development of a talik. The spread of ALT for the individual scenarios increases towards the end of the period and depends on assumed water/ice content (Fig. 5c). Apart from Gruvefjellet, taliks develop at all other sites for GST scenarios above the 75% percentile.

6. Model results show degradation of permafrost in bedrock sites at low elevations. Contrarily, in sedimentary landforms with a relatively high water/ice content, modelled ground temperatures increase to close to 0 °C, but permafrost conditions continue to exist until 2100.

7. During 2000 and 2009 we have an overlap between scenario and instrumental data at the Janssonhaugen site. The ALT modelled based on the scenario median slightly overestimates modelled ALT when using observed GSTs (Fig. 5d).

4.3 Sensitivity to changes in seasonal air temperature

A sensitivity analysis was conducted for the study sites, addressing the effect of temperature changes in different seasons. This was achieved by attenuating the amplitudes above and below 0 °C, respectively, of the GST by a factor between 0 and 1, and extracting the associated ground temperature at 15 m depth and the active layer thicknesses (Fig. 7). The results suggest for a given temperature change that an increase of winter temperature and/or increase of snow cover has a major effect on warming the permafrost, while an increase in summer temperature mainly affects the ALT. However, also the warming during winter affects the ALT. The bedrock sites had a more rapid response both with respect to ALT and ground temperature because of a low water/ice content, with especially quick reactions in the Kapp Linné BH1 site.

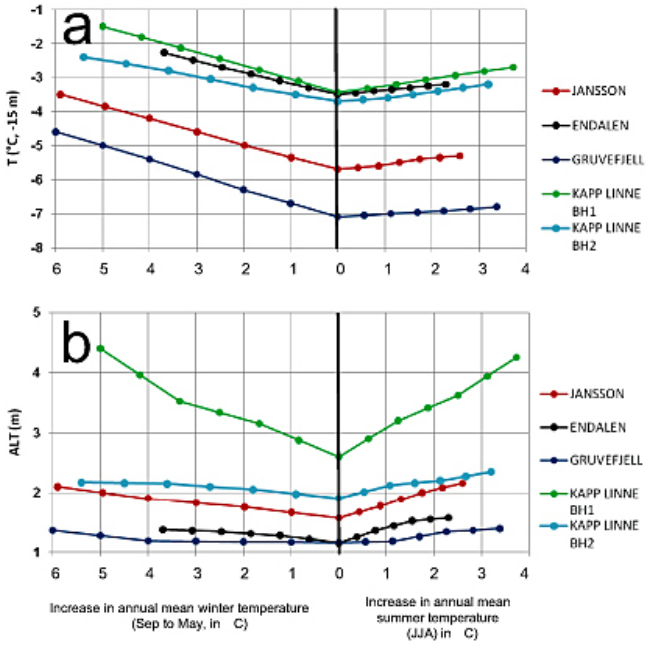

Fig. 7. Impact of GST changes during summer (JJA) and fall/winter/spring (September to May) on ground temperature in 15 m depth **(a)** and on ALT **(b)** for the different study sites. The model was then run over a period of 10 years and the presented results are the differences to the undisturbed values.

5 Discussion

5.1 Uncertainties and sensitivity

The major uncertainties for this study are related to (1) deficits of the heat conduction model, (2) the spread of the SAT-scenario ensemble and (3) the validity of the statistical relationships between SAT at Svalbard Airport and the GST at the borehole sites and (4) lack of detailed knowledge of ice content, stratigraphy and other geophysical parameters through the permafrost, as no cores could be obtained when establishing the boreholes.

The heat flow model used in this study does not account for annual or inter-annual variations of water content in the active layer layers, like other model approaches do (e.g. Zhang et al., 2003; Burn and Zhang, 2009). However, the model performed well during calibration, even in the ice-rich site of Endalen. This behaviour is probably related to the generally low water content in the relatively coarse sediments above bedrock and pure bedrock at the borehole sites. Over the period 1912–2000, precipitation has increased (Hanssen-Bauer and Førland, 1998; Førland and Hanssen-Bauer, 2000, 2003) and a further ∼5% increase is expected based on the GCM scenarios (Benestad, 2008; Hanssen-Bauer, 2007). Such an increase in precipitation would furthermore increase the water content of the active layer, depending on snow redistribution. However, thicker active layers would release water from thawing of the transient layer (Shur et al., 2005), which is ice-rich. On the other hand, an increase in ALT and thawing of ground ice may decrease the water content. It is obvious that the drying of the active layer may lead to non-linear responses of the thermal regime, typically intensifying the increase in temperature, as already observed in mountain sites in southern Norway (Farbrot et al., 2011; Isaksen et al., 2011). In our study this is demonstrated for the two Kapp Linné sites, which show a different response for the ALT projections due to differences in assumed water/ice content. Thus, our estimates here are considered as rather conservative.

Large uncertainties are related to the spread between the individual SAT scenarios. This spread is about 4–6 °C and is larger than uncertainties related to the heat flow model in terms of water/ice content evolution. We suggest, that the median of the resultant temperature distribution is a realistic indication of the future evolution given the used temperature

scenarios. However, the variability of the individual scenarios contains information about the thermal responses in the ground, reflecting soil properties and moisture conditions. At sites where temperatures approach 0 °C, the spread is reduced due to the consumption of latent heat associated with thawing, e.g. the Endalen site. This is in accordance with observed warming trends recently published e.g. by Romanovsky et al. (2010a) and Smith et al. (2010) from Russia and North America, respectively.

The coupling between SAT at Svalbard Airport and GST at the individual sites depends strongly on snow cover thickness and duration. Here, we have derived GST series from SAT using n-factors, implicitly assuming unchanged snow conditions over the considered period. This may seem somewhat unrealistic given the pronounced warming, especially during winter. A general reduction in snow cover duration would lead to a reduced warming of the ground since the heat loss of the ground would be enhanced during the cold period. On the other hand, a thinner snow cover also has a tendency to disappear earlier in spring time, possibly leading to subsurface warming earlier and during a longer time interval. Recent studies highlight the effect of snow cover thickness and duration on ground temperatures (e.g. Lütschg et al., 2008), while Engelhardt et al. (2010) showed that differences in the timing of a thick snow cover have a similar influence on ground temperature as different forcing climate scenarios. Recently, Christiansen et al. (2010) and Romanovsky et al. (2010b) demonstrated the large differences of near-surface ground temperatures between two adjacent boreholes with different snow cover in Svalbard. Deeper ground temperatures will, however, become more similar because of the lateral heat transfer, causing temperatures at greater depths to be integrated over larger surface areas. In our study, however, the values of the n_F-factors are close to 1 besides for the Endalen site, indicating little influence of snow on the SAT-GST coupling. Further, the anticipated warming would on a longer time-scale cause higher vegetation stands like bushes, thereby altering the n_T-factors. This would lead to more snow becoming potentially trapped, increasing the GST during winter, even if summer GST would decrease because of increased shading (e.g. Blok et al., 2010; Sharkhuu et al., 2007; Hinzman et al., 2005).

Finally, the SAT-GST relationships employed here assume a constant lapse rate between Svalbard Airport and the study sites of $0.0065\,^{\circ}\mathrm{C\,m^{-1}}$. The mean annual lapse rates during our measurement period in this study was 0.006–$0.007\,^{\circ}\mathrm{C\,m^{-1}}$ between Svalbard Airport and the stations on Janssonhaugen and Gruvefjellet (average 2000–2010 was $0.0062\,^{\circ}\mathrm{C\,m^{-1}}$) , respectively. However, lapse rates are not constant over time and especially at high Arctic coastal sites highly depending on sea ice and the local air flow conditions. Svalbard Airport is situated at the coast, and its air temperature, especially during winter, is largely affected by sea ice cover. The station is highly sensitive to the coupled sea ice-ocean-atmosphere system (Benestad et al., 2002) and recently observed shrinkage in Arctic sea-ice cover (Vinje, 2001; Stroeve et al., 2007) suggests that larger differences may be expected further inland e.g. at Endalen, Gruvefjellet and Janssonhaugen today than previously (O. Humlum, personal communication, 2010).

In summary, different uncertainties draw in different directions, and the importance of each factor is difficult to quantify or even unknown. We believe, however, that our results provide a fairly realistic picture of consequences of future CO_2-emissions as specified in the A1b scenario.

5.2 Trends and consequences

According to the model the warming since the start of the last century has resulted in a low-gradient temperature profile, which corresponds well with the measured values. We model a ca. +0.5 °C difference between modelled and measured GT at 20 m depth for the Janssonhaugen site, while the overall gradient fits well. The offset is probably due to two main reasons. First, the initial temperature distribution is somewhat speculative and temperature may have been too low, as the former ground temperature history is not known. Secondly, lapse rates may have differed during earlier parts of the last century as mentioned above. For all sites the modelled active layer thicknesses correspond to the measured values from the boreholes within ca. ± 0.3 m.

During the last 100 years only minor changes occurred in the modelled ground temperatures, apart from the period since the mid 1990s which were the warmest since the instrumental record started. The last 10–15 years warming can explain almost 50% of the simulated warming in the uppermost 50 m of the permafrost. We clearly see the warm year of 2006/2007, described and analysed in Isaksen et al. (2007a), with a considerable increase in ALT at all sites apart from Gruvefjellet. Individual warm events like that in spring 2006 are important, as the system needs time to recover, as e.g. demonstrated for the Alps after a similar event in 2003 (cf. Hilbich et al., 2008; Gruber et al., 2004). In general, the active layer change during recent years, and especially during the last decades is similar to observations in other parts of the world (Romanovsky et al., 2010a; Smith et al., 2010; Zhao et al., 2010; Christiansen et al., 2010).

In Svalbard the air temperature variability during summer and winter is different. While summer temperatures are fairly constant between years, the variability of winter temperature is high (Førland et al., 2009). The trends for the entire instrumental SAT record at Svalbard Airport (1912–2009) show that temperatures have increased significantly during spring (MAM, $+0.044^{\circ}\,\mathrm{C\,a^{-1}}$), winter (DJF, $+0.015^{\circ}\,\mathrm{C\,a^{-1}}$) and autumn (SON, $+0.014^{\circ}\,\mathrm{C\,a^{-1}}$), whereas summer (JJA, $+0.009^{\circ}\,\mathrm{C\,a^{-1}}$) temperatures were more constant during the last century (Førland et al., 2009). Our sensitivity study suggests that the increase of winter temperatures leads to a substantial warming of the permafrost, while the relatively constant summer temperatures have only a minor influence and

mainly on the active layer thickness. This explains the low variability of the modelled ALT during large parts of the last century. An exception is the bedrock site at Kapp Linné BH1, which shows a somewhat faster response also in ALT when winter temperature increases.

For the future development, the ground thermal regime stays relatively stable for reasons discussed above. However, sites close to sea level are modelled to undergo some permafrost degradation and thus to develop taliks above the remaining permafrost. The major effect is the warming of the permafrost, where temperatures are modelled to rise to above −2 °C at 20 m depth in the more continental sites and above −1 °C at the lower sites like Endalen and Kapp Linné. Such temperature conditions are currently observed within the discontinuous mountain permafrost in e.g. the high mountains of the Norwegian mainland (Christiansen et al., 2010; Farbrot et al., 2011).

5.3 Geomorphological implications

Major permafrost changes are mainly to be expected by the end of the 21st century in areas where the permafrost is warmest at present. This includes areas situated generally in the lower parts of the landscape, such as along the coast lines and in the outer parts of the large glacial valleys of Nordenskiöldland (Fig. 8) below 100 m a.s.l., where the local settlements exist. These areas are characterized by the presence of mainly marine, raised beach sediments, fluvial and glaciofluvial sediments, partly overlain by eolian, colluvial or alluvial deposits, having a relatively fine matrix (Christiansen et al., 2010). Those sediments are ice-rich, and associated periglacial landforms such as ice wedges, pingos and solifluction sheets or lobes are wide-spread (Christiansen, 2005; Harris et al., 2009; Ross et al., 2007). However, the permafrost thermal snapshot obtained during 2008–2010 from fine-grained sediment landforms in lower Adventdalen, also showed significantly colder permafrost of −5 °C to −6 °C at the depth of ZAA (Christiansen et al., 2010), most likely due to a combination of cold air drainage through these valleys with generally thin snow cover and high ice content. Thus, addressing the consequences of climate change on certain periglacial processes remains a challenge. The possible thaw of the ice-rich layers in the transition zones on the top of permafrost has received considerable attention (Büdel, 1982; Shur et al., 2005; Murton et al., 2006). On one hand, this effect buffers ground warming, on the other hand it may cause a non-linear ground temperature response if completely thawed. Resulting increases in ALT may in certain areas of Svalbard be associated with unprecedented thaw settlement as ice-rich soils thaw (Nelson et al., 2001), and in consequence, a marked increase in slope instability (Harris et al., 2001, 2009; Davis et al., 2001; Gruber and Haeberli, 2007). An important geomorphological consequence for bedrock in coastal areas is coastal erosion. The coastal sections within the study areas have a high frequency of rock cliffs (e.g. Etzelmüller et al., 2003; Ødegård et al., 1987) formed in sedimentary bedrock. Those are heavily shattered by frost weathering, and presumably an important source for coastal material transport and erosion (e.g. Ødegård et al., 1995; Ødegård and Sollid, 1993). Such sites would be highly susceptible to the anticipated changes, assuming that many cliffs are stabilized by permafrost.

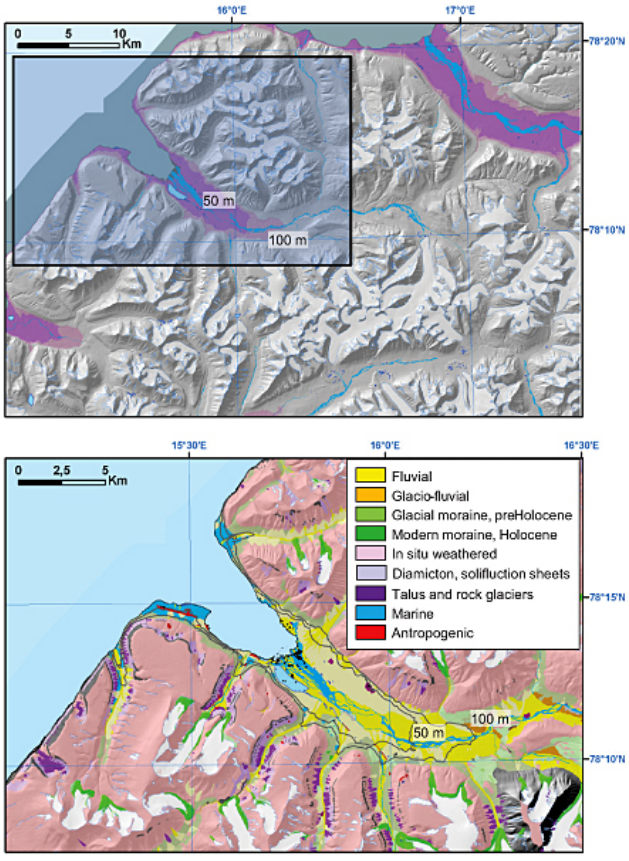

Fig. 8. Upper panel: hillshaded map of the Adventdalen area and surroundings. The two purple colours denote the 50 m and 100 m elevation contour, respectively. Large areas within the valley bottoms draining to Isfjorden are laying within this zone. Lower panel: geomorphological map over the area around Longyearbyen (based on Tolgensbakk et al., 2000). The gray lines denote the contours from above. The area below 50 m is mainly covered by marine sediments, beach deposits, fluvial infilling, slope sediment such as gelifluction colluviums, alluvial fans and some singular bedrock outcrops, mainly in steep rock walls or coastal cliffs.

6 Conclusions

From this study the following conclusions are drawn:

– The substantial warming of ground temperatures and associated active layer thickening observed in recent years on Janssonhaugen was successfully reproduced by a heat conduction model.

- Since the end of the Little Ice Age on Svalbard (mid to end of 19st century) and until 1990, permafrost has warmed by around 1 °C and since then by 0.5–1 °C. There was little variation in modelled ALT over these 100 years although there was substantial variability of air temperature. MAAT changes were mainly caused by the increase of winter temperatures and thus have less influence on ALT.

- A similar pattern is modelled for the future, with a general warming of permafrost, but limited changes in the ALT, at least at ice-rich sites.

- The sensitivity analysis shows that ground temperatures are more sensitive to changes in winter temperatures than to changes in summer temperatures for sites with a sediment cover. Changes in summer temperatures have a direct impact on ALT, whereas ALT is only indirectly affected by changes in winter temperatures through the general influence on ground temperatures.

- Permafrost degradation can be expected at low elevations, e.g. close to the coast below ca. 100 m a.s.l. in well-drained and dry sites (e.g. bedrock), where taliks likely can develop. From this analysis a major degradation of permafrost is not expected on Svalbard during the next ca. 50 years for areas with no ground disturbances by human activity.

Acknowledgements. This study was funded by the Norwegian Research Council, project no. 176033/S30 (Permafrost Observatory Project: a Contribution to the Thermal State of Permafrost in Norway and Svalbard) and 185987/V30 (CRYOLINK – Permafrost and seasonal frost in Southern Norway: understanding and modelling the atmosphere-ground temperature), the University of Oslo, Norway, the University Centre of Svalbard (UNIS), the Norwegian Meteorological Institute, Oslo, and the Geological Survey of Norway, Trondheim. The manuscript was greatly improved by the comments of Wilfried Haeberli and two anonymous reviewers. The map of Fig. 1 was made by Markus Eckerstorfer (UNIS), based on digital map data provided by the Norwegian Polar Institute (NP). We want to thank all mentioned individuals and institutions.

Edited by: D. Riseborough

References

Aagaard, K. and Carmack, E. C.: The Role of Sea Ice and Other Fresh-Water in the Arctic Circulation, J. Geophys. Res.-Oceans, 94, 14485–14498, 1989.

ACIA: Arctic Climate Impact Assessment, Cambridge University Press, Cambridge, UK, 1042 pp., 2005.

Benestad, R. E.: A comparison between two empirical downscaling strategies, Int. J. Climatol., 21, 1645–1668, 2001.

Benestad, R. E.: Climate change scenarios for northern Europe from multi-model IPCC AR4 climate simulations, Geophys. Res. Lett., 32, L17704, doi:10.1029/2005gl023401, 2005.

Benestad, R. E.: Empirical-Statistical downscaled Arctic Temperature and precipitation, Series, Met. no Report 12/2008 Climate, Norwegian Meteorological Institute, Oslo, 2008.

Benestad, R. E.: A new global set of downscaled temperature scenarios, J. Climate, doi:10.1175/2010JCLI3687.1, in press, 2011.

Benestad, R. E., Førland, E. J., and Hannssen-Bauer, I.: Empirically downscaled temperature scenarios for Svalbard, Atmos. Sci. Lett., 3, 71–93, 2002.

Blok, D., Heijmans, M. M. P. D., Schaepman-Strub, G., Kononov, A. V., Maximov, T. C., and Berendse, F.: Shrub expansion may reduce summer permafrost thaw in Siberian tundra, Glob. Change Biol., 16, 1296–1305, 2010.

Burn, C. R. and Zhang, Y.: Permafrost and climate change at Herschel Island (Qikiqtaruq), Yukon Territory, Canada, J. Geophys. Res.-Earth, 114, F02001, doi:10.1029/2008JF001087, 2009.

Büdel, J.: Climatic Geomorphology, Princeton University Press, Princeton, 443 pp., 1982.

Christiansen, H. H.: Thermal regime of ice-wedge cracking in Adventdalen, Svalbard, Permafrost Periglac., 16, 87–98, 2005.

Christiansen, H. H., Etzelmüller, B., Isaksen, K., Juliussen, H., Farbrot, H., Humlum, O., Johansson, M., Ingeman-Nielsen, T., Kristensen, L., Hjort, J., Holmlund, P., Sannel, A. B. K., Sigsgaard, C., Akerman, H. J., Foged, N., Blikra, L. H., Pernosky, M. A., and Odegard, R. S.: The Thermal State of Permafrost in the Nordic Area during the International Polar Year 2007–2009, Permafrost Periglac., 21, 156–181, doi:10.1002/Ppp.687, 2010.

Davis, M. C. R., Hamza, O., and Harris, C.: The effect of rise in mean annual temperature on the stability of rock slopess containing ice-filled discontinuities, Permafrost Periglac., 12, 137–144, 2001.

Engelhardt, M., Hauck, C., and Salzmann, N.: Influence of atmospheric forcing parameters on modelled mountain permafrost evolution, Meteorol. Z., 19(5), 491–500, doi:10.1127/0941-2948/2010/0476, 2010.

Etzelmüller, B., Ødegård, R. S., and Sollid, J. L.: The spatial distribution of coast types on Svalbard, in: Arctic Coastal Dynamics – Reports of the 3rd International Workshop, University of Oslo (Norway), 2–5 December 2002, edited by: Rachold, V., Brown, J., Solomon, S., and Sollid, J. L., Reports on Polar and Marine Research, Alfred Wegener Institute for Polar and Marine Research, Bremerhaven, 33–40, 2003.

Farbrot, H., Etzelmüller, B., Gudmundsson, A., Schuler, T. V., Eiken, T., Humlum, O., and Björnsson, H.: Thermal characteristics and impact of climate change on mountain permafrost in Iceland, J. Geophys. Res., 112, F03S90, doi:10.1029/2006JF000541, 2007.

Farbrot, H., Etzelmüller, B., Hipp, T., Isaksen, K., Ødegård, R. S., Schuler, T. V., and Humlum, O.: Air and ground temperature variations observed along elevation and continental gradients in Southern Norway, Permafrost Periglac., submitted, 2011.

French, H. M.: The periglacial environment, 2nd edn., Longmann, London, 341 pp., 1996.

Førland, E. J. and Hanssen-Bauer, I.: Increased precipitation in the Norwegian Arctic: True or false?, Climatic Change, 46, 485–509, 2000.

Førland, E. J. and Hannssen-Bauer, I.: Past and future climate variations in the Norwegian Arctic: overview and novel analyses, Polar Res., 22, 113–124, 2003.

Førland, E. J., Benestad, R. E., Flatøy, F., Hanssen-Bauer, I.,

Haugen, J. E., Isaksen, K., Sorteberg, A., and Aadlandsvik, B.: Climate development in North Norway and the Svalbard region during 1900–2100, Norwegian Polar Institute, Tromsø, 44 pp., 2009.

Goodrich, L. E.: The influence of snow cover on the ground thermal regime, Can. Geotech. J., 19, 421–432, 1982.

Gruber, S. and Haeberli, W.: Permafrost in steep bedrock slopes and its temperature-related destabilization following climate change, J. Geophys. Res.-Earth, 112, F02s18, doi:10.1029/2006jf000547, 2007.

Gruber, S., Hoelzle, M., and Haeberli, W.: Permafrost thaw and destabilization of Alpine rock walls in the hot summer of 2003, Geophys. Res. Lett., 31, L13504, doi:10.1029/2004gl020051, 2004.

Hanssen-Bauer, I.: Climate variation in the European sector of the Arctic: Observations and scenarios, in: Arctic-Alpine Ecosystems and people in a Changing Environment, edited by: Orb, J. B. E. A., Springer Verlag, Hamburg, 2007.

Hanssen-Bauer, I. and Førland, E. J.: Long-term trends in precipitation and temperature in the Norwegian Arctic: can they be explained by changes in atmospheric circulation patterns?, Climate Res., 10, 143–153, 1998.

Harris, C., Davis, M., and Etzelmüller, B.: The Assessment of Potential Geotechnical Hazard Associated With Mountain Permafrost in a Warming Global Climate, Permafrost Periglac., 12, 145–156, 2001.

Harris, C., Arenson, L. U., Christiansen, H. H., Etzelmüller, B., Frauenfelder, R., Gruber, S., Haeberli, W., Hauck, C., Holzle, M., Humlum, O., Isaksen, K., Kaab, A., Kern-Lutschg, M. A., Lehning, M., Matsuoka, N., Murton, J. B., Nozli, J., Phillips, M., Ross, N., Seppala, M., Springman, S. M., and Mühll, D. V.: Permafrost and climate in Europe: Monitoring and modelling thermal, geomorphological and geotechnical responses, Earth-Sci. Rev., 92, 117–171, doi:10.1016/j.earscirev.2008.12.002, 2009.

Hilbich, C., Hauck, C., Hoelzle, M., Scherler, M., Schudel, L., Voelksch, I., Mühll, D. V., and Maeusbacher, R.: Monitoring mountain permafrost evolution using electrical resistivity tomography: A 7-year study of seasonal, annual, and long-term variations at Schilthorn, Swiss Alps, J. Geophys. Res.-Earth, 113(F1), F01S90, doi:10.1029/2007JF000799, 2008.

Hinzman, L. D., Bettez, N. D., Bolton, W. R., Chapin, F. S., Dyurgerov, M. B., Fastie, C. L., Griffith, B., Hollister, R. D., Hope, A., Huntington, H. P., Jensen, A. M., Jia, G. J., Jorgenson, T., Kane, D. L., Klein, D. R., Kofinas, G., Lynch, A. H., Lloyd, A. H., McGuire, A. D., Nelson, F. E., Oechel, W. C., Osterkamp, T. E., Racine, C. H., Romanovsky, V. E., Stone, R. S., Stow, D. A., Sturm, M., Tweedie, C. E., Vourlitis, G. L., Walker, M. D., Walker, D. A., Webber, P. J., Welker, J. M., Winker, K., and Yoshikawa, K.: Evidence and implications of recent climate change in northern Alaska and other arctic regions, Climatic Change, 72, 251–298, 2005.

Humlum, O., Instanes, A., and Sollid, J. L.: Permafrost in Svalbard: a review of research history, climatic background and engineering challenges, Polar Res., 22, 191–215, 2003.

Isaksen, K., Vonder Mühll, D., Gubler, H., Kohl, T., and Sollid, J. L.: Ground surface temperature reconstruction based on data from a deep borehole in permafrost at Janssonhaugen, Svalbard, Ann. Glaciol., 31, 287–294, 2000.

Isaksen, K., Benestad, L. E., Harris, C., and Sollid, J. L.: Recent extreme near-surface permafrost temperatures on Svalbard in relation to future climate scenarios, Geophys. Res. Lett., 34, L17502, doi:10.1029/2007GL031002, 2007a.

Isaksen, K., Sollid, J. L., Holmlund, P., and Harris, C.: Recent warming of mountain permafrost in Svalbard and Scandinavia, J. Geophys. Res.-Earth, 112(F2), F02S04, doi:10.1029/2006JF000522, 2007b.

Isaksen, K., Ødegård, R. S., Etzelmüller, B., Hilbich, C., Hauck, C., Farbrot, H., Eiken, T., Hygen, H. O., and Hipp, T.: Degrading mountain permafrost in southern Norway – spatial and temporal variability of mean ground temperatures 1999–2009, Permafrost Periglac., submitted, 2011.

Juliussen, H., Christiansen, H. H., Strand, G. S., Iversen, S., Midttømme, K., and Rønning, J. S.: NORPERM, the Norwegian Permafrost Database – a TSP NORWAY IPY legacy, Earth Syst. Sci. Data Discuss., 3, 27–54, doi:10.5194/essdd-3-27-2010, 2010.

Lachenbruch, A. H. and Marshall, B. V.: Changing climate: geothermal evidence from permafrost in the Alaskan Arctic., Science, 234, 689–696, 1986.

Liestøl, O.: Pingos, springs, and permafrost in Spitsbergen, Norsk Polarinstitutt Årbok, 1975, 7–29, 1977.

Lütschg, M., Lehning, M., and Haeberli, W.: A sensitivity study of factors influencing warm/thin permafrost in the Swiss Alps, J. Glaciol., 54, 696–704, 2008.

Meehl, G. A., Covey, C., Delworth, T., Latif, M., McAvaney, B., Mitchell, J. F. B., Stouffer, R. J., and Taylor, K. E.: The WCRP CMIP3 multimodel dataset – A new era in climate change research, B. Am. Meteorol. Soc., 88, 1383, doi:10.1175/Bams-88-9-1383, 2007.

Murton, J. B., Peterson, R., and Ozouf, J. C.: Bedrock fracture by ice segregation in cold regions, Science, 314, 1127–1129, 2006.

Nelson, F. E., Anisimov, O. A., and Shiklomanov, N. I.: Subsidence risk from thawing permafrost – The threat to man-made structures across regions in the far north can be monitored, Nature, 410, 889–890, 2001.

Nordli, Ø. and Kohler, J.: The early 20th century warming, Daily observations at Grønfjorden and Longyearbyen on Spitsbergen, 2nd edn., Norwegian Meteorlogical Institute, Oslo, 2004.

Ødegård, R. and Sollid, J. L.: Coastal cliff temperatures related to the potential for cryogenic weathering processes, western Spitsbergen, Svalbard, Polar Res., 12, 95–106, 1993.

Ødegård, R., Etzelmüller, B., Vatne, G., and Sollid, J. L.: Near-surface spring temperatures in an Arctic coastal rock cliff: Possible implications for rock breakdown, in: Steepland Geomorphology, edited by: Slaymaker, O., Wiley, Chichester, 89–102, 1995.

Ødegård, R. S., Sollid, J. L., and Trollvik, J. A.: Kystkart Svalbard A3 Forlandsundet 1:200 000, Norsk Polarinstitutt and Unviersity of Oslo, Oslo, 1987.

Romanovsky, V. E., Drozdov, D. S., Oberman, N. G., Malkova, G. V., Kholodov, A. L., Marchenko, S. S., Moskalenko, N. G., Sergeev, D. O., Ukraintseva, N. G., Abramov, A. A., and Vasiliev, A. A.: Thermal state of permafrost in Russia, Permafrost Periglac., 22, 136–155, 2010a.

Romanovsky, V. E., Smith, S. L., and Christiansen, H. H.: Permafrost Thermal State in the Polar Northern Hemisphere during the International Polar Year 2007–2009: a Synthesis, Permafrost Periglac., 21, 106–116, doi:10.1002/Ppp.689, 2010b.

Ross, N., Brabham, P. J., Harris, C., and Christiansen, H. H.: Internal structure of open system pingos, Adventdalen, Svalbard: The use of resistivity tomography to assess ground-ice conditions, J. Environ. Eng. Geoph., 12, 113–126, 2007.

Sengupta, S. and Boyle, J. S.: Using Common Principal Components in Comparing GCM Simulations, J. Climate, 11, 816–830, 1998.

Sharkhuu, A., Sharkhuu, N., Etzelmüller, B., Heggem, E. S. F., Nelson, F. E., Shiklomanov, N., Goulden, C., and Brown, J.: Permafrost Monitoring in the Hovsgol Mountain Region, Mongolia, J. Geophys. Res., 112(F2), F02S06, doi:10.1029/2006JF000543, 2007.

Shur, Y., Hinkel, K. M., and Nelson, F. E.: The transient layer: Implications for geocryology and climate-change science, Permafrost Periglac., 16, 5–17, 2005.

Smith, M. W. and Riseborough, D. W.: Climate and the limits of permafrost: A zonal analysis, Permafrost Periglac., 13, 1–15, 2002.

Smith, S. L., Romanovsky, V. E., Lewkowicz, A. G., Burn, C. R., Allard, M., Clow, G. D., Yoshikawa, K., and Throop, J.: Thermal state of permafrost in North America – a contribution to the International Polar Year, Permafrost Periglac., 22, 117–135, 2010.

Solomon, S., Quin, D., Manning, M., Chen, Z., Marquis, M., Averyt, K. B., Tignotr, M., and Miller, H. L.: Climate Change: The Physical Science Basis. Contribution of Working Group I to the Fourth Assessment Report of the Intergovernmental Panel on Climate Change, Cambridge University Press, UK and New York, NY, USA, 2007.

Strang, G.: Linear Algebra and its Application, Harcourt Brace and Company, San Diego, California, USA, 1988.

Stroeve, J., Holland, M. M., Meier, W., Scambos, T., and Serreze, M.: Arctic sea ice decline: Faster than forecast, Geophys. Res. Lett., 34(9), L09501, doi:10.1029/2007GL029703, 2007.

Tolgensbakk, J., Sørbel, L., and Høgvard, K.: Geomorphological and quarternary geological map 1:100 000 Sheet C9Gq Adventdalen, Nor. Polarinst. Temakart 32, 2000.

Uppala, S. M., Kallberg, P. W., Simmons, A. J., Andrae, U., Bechtold, V. D., Fiorino, M., Gibson, J. K., Haseler, J., Hernandez, A., Kelly, G. A., Li, X., Onogi, K., Saarinen, S., Sokka, N., Allan, R. P., Andersson, E., Arpe, K., Balmaseda, M. A., Beljaars, A. C. M., Van De Berg, L., Bidlot, J., Bormann, N., Caires, S., Chevallier, F., Dethof, A., Dragosavac, M., Fisher, M., Fuentes, M., Hagemann, S., Holm, E., Hoskins, B. J., Isaksen, L., Janssen, P. A. E. M., Jenne, R., McNally, A. P., Mahfouf, J. F., Morcrette, J. J., Rayner, N. A., Saunders, R. W., Simon, P., Sterl, A., Trenberth, K. E., Untch, A., Vasiljevic, D., Viterbo, P., and Woollen, J.: The ERA-40 re-analysis, Q. J. Roy. Meteor. Soc., 131, 2961–3012, 2005.

Vinje, T.: Anomalies and trends of sea-ice extent and atmospheric circulation in the Nordic Seas during the period 1864–1998, J. Climate, 14, 255–267, 2001.

Wegmann, M., Gudmundsson, G. H., and Haeberli, W.: Permafrost changes in rock walls and the retreat of alpine glaciers: A thermal modelling approach, Permafrost Periglac., 9, 23–33, 1998.

Wilks, D. S.: Statistical Methods in the Atmospheric Sciences, Academic Press, Orlando, Florida, USA, 1995.

Williams, P. J. and Smith, M. W.: The Frozen Earth: Fundamentals of geocryology, Cambridge University press, Cambridge, 300 pp., 1989.

Zhang, Y., Chen, W. J., and Cihlar, J.: A process-based model for quantifying the impact of climate change on permafrost thermal regimes, J. Geophys. Res.-Atmos., 108(D22), 4695, doi:10.1029/2002JD003354, 2003.

Zhao, L., Wu, Q., Marchengo, S., and Sharkhuu, N.: Thermal state of permafrost and active layer in Central Asia during the International Polar Year, Permafrost Periglac., 22, 198–207, 2010.